Thermal study during milling of Ti6Al4V produced by Electron Beam Melting (EBM) process

Samuel Milton, Arnaud Duchosal, Florent Chalon, René Leroy, Antoine Morandeau

Title:

Thermal study during milling of Ti6Al4V produced by Electron Beam Melting (EBM) process

Authors:

Samuel Milton [1,2,*], Antoine Morandeau [2], Arnaud Duchosal [1], Florent Chalon [1], René Leroy [1]

Affiliations:

[1] Université de Tours, Université d'Orléans, INSA LVL, Laboratoire de Mécanique Gabriel Lamé, Tours, France.

[2]Sandvik Tooling Division Coromant, R&D, Fondettes, France.

Corresponding author: Tel.: +33 (0)2 47 62 52 59; E-mail address: samuelmilton02@gmail.com

Title

Thermal study during milling of Ti6Al4V produced by Electron Beam Melting (EBM) process.

Abstract

Electron Beam Melting (EBM) process, an additive manufacturing technique is now used to make real functional parts and these parts need finish machining to ensure better surface quality. Temperature rise is one of the main factors that determine the productivity in the metal cutting industry. This study was aimed at determining the differences in temperature and forces at the cutting zone along with heat partition at the tool-material interface while milling Ti6Al4V produced by EBM processes when compared to Ti6Al4V produced by conventional lamination process. An innovative hybrid approach was used to determine the heat flux and study the effects of temperature using both milling and tribological experiments. Milling was done under finishing conditions with a feed rate of 0.1 mm/tooth and cutting speed of 50 m/min. Ti6Al4V produced by EBM process generated about twice the heat flux that enters the cutting tool and leads to 50% lower tool life when compared to the one produced by the conventional hot rolling process which was used as a reference. This change in thermal behavior is attributed to the differences in the microstructure of Ti6Al4V based on the corresponding process routes which modified the type tool-material interactions and wear mechanisms. Results provide a better understanding of the thermal effects while milling EBM-Ti6Al4V and prove that cutting conditions have to be optimized to ensure higher material removal rates and better surface integrity of the parts.

Keywords:

Electron Beam Melting (EBM), Temperature, Heat partition, Milling, Ti6Al4V

Nomenclatures

ϕ_{Tool}	Total heat flux transmitted to the cutting tool [w]
ϕ_{Shear}	Part of the heat entering the tool due to shearing of the workpiece [w]
$\phi_{Friction}$	Part of the heat due to frictional effect [w]
$\phi_{rake\ face}$	The heat produced in the secondary and tertiary zones transmitted to the tool through the rake face [w]
$\phi_{flank\ face}$	The heat produced in the secondary and tertiary zones transmitted to the tool through the flank face [w]
N_R	The normal force on the rake face [N]
N_F	The normal force on the flank face [N]
T_R	The tangential force on the rake face [N]
T_F	The tangential force on the flank face [N]
μ_R	The apparent coefficient of friction experienced at the rake face
μ_F	The apparent coefficient of friction experienced at the flank face
μ_{app}	Apparent coefficient of friction
V_C	Cutting Speed [m/min]
V_f	Feed rate [m/min]
a_p	Depth of cut [mm]

A_R	The contact surface area at rake face [m²]
A_f	The contact surface area at flank face [m²]
B	Heat partition coefficient
K_r	Insert entering angle [°]
H_{ex}	Maximum chip thickness [mm]
γ_n	Effective rake angle [°]
V_b	Flank wear [mm]
P_{total}	The total power consumed by friction of the pin [w]
Φ_{pin}	Heat flux entering the pin [w]
k	Thermal conductivity [w/m.K]
S_{pin}	Cross sectional area of the pin [mm²]
$\Delta T/dx$	The temperature gradient in the pin [K/mm]
F_t	Apparent tangential force in the pin [N]
V_s	Sliding velocity [m/min]
$\beta_{pin-disc}$	The ratio of the heat flux entering the pin to the total power consumed by friction

1. Introduction

Ti6Al4V alloy is widely used in aerospace and medical sectors mainly due to their high strength to weight ratio and biocompatibility [1,2]. In the present era of material processing, additive manufacturing (AM) is taking over the traditional manufacturing processes due to its advantage in reducing the material usage and carbon footprint. New aircraft parts were being designed using AM techniques like Electron Beam Melting (EBM), Selective Laser Melting (SLM) etc. In spite of the benefits of making complex designs and lesser material waste, the final surface finish obtained with the EBM process has an average roughness of 10 – 30µm [3]. To generate the functional surface with close tolerances of < 0.5 µm, CNC machining is needed. The parts built with AM are produced as near net shaped with an allowance for final machining under finishing conditions. Combining the AM processes and the subtractive techniques offer benefits of both the technologies and is economically viable.

Temperature rise during the cutting process plays a vital role in optimizing the cutting conditions due to its effect on tool life and the material removal rate [4]. Moreover, machinability of Ti6Al4V is generally considered to be poor due to its low thermal conductivity, elastic modulus, and chemical reactivity [4][5]. Due to its low thermal conductivity, the temperature rise in the cutting tool can reach up to 1000°C for Ti6Al4V alloys [6]. This high-temperature rise is undesirable, as it reduces the tool life and degrades the surface integrity of the work-piece. It is important to understand the effect of temperature at the cutting edge of the tool while machining the EBM produced Ti6Al4V in order to estimate the tool life and the surface integrity of the part [7][8]. During the machining process, the main part of cutting energy is transformed into heat and is dissipated into the chip, tool, and the work-piece material due to shearing and friction that generate heat. Needless to say, the maximum productivity can be achieved only by optimizing the cutting conditions based on the minimized heat in the cutting zone. Measuring temperature at the cutting edge is difficult due to the reduced access to the cutting zone. Though several articles have been published regarding the temperature rise in turning operation [9–11], milling being an intermittent cutting process has received substantially lesser attention.

Several experimental techniques like embedded thermocouples, direct radiance measurement system etc. have been used [6], [12–14]. However studying the thermal effects along with understanding the tribological phenomena at the tool-chip contact has always been

a challenge due to reduced access to the sliding zones during actual cutting process. To overcome this difficulty, researchers have developed controllable laboratory tests where the conditions of sliding could be accurately measured [15–18]. Most widely used set-up is pin-on-disc test where a pin with a spherical head made of the the cutting tool material is slid over the surface of the work-piece material made in the form of disc. Pin on disc tests were done to replicate the contact conditions at tool-material interface during chip formation in the cutting process and deterimine the heat partition at the interface. In this experimental set-up contact pressures and the sliding velocities could be controlled while the sliding forces and the temperature rise during sliding can be measured.

In this study, a novel hybrid approach was used to estimate the heat flux entering the tool from the cutting zone while milling Ti6Al4V produced by EBM process. The hybrid approach combines both milling and tribological tests (pin on disc) to estimate the heat flux transmitted into the cutting tool. Tool lifetime tests are done to study the evolution of the wear at the cutting edge. The effect of the temperature rise reflects directly on the lifetime of the tool. A conventionally laminated Ti6Al4V alloy is used as a reference material all through the study to compare the results. This study brings a broader understanding of the sources of heat affecting the temperature rise and in turn its lifetime. This will help in optimizing the cutting conditions as well as in the development of new cutting tools to machine the EBM parts in the future.

2. Theory and Methodology

2.1 Heat distribution theory during machining

During metal cutting, heat is generated from three main shear zones as represented in Figure 1. The primary source is when tool shears the workpiece material against its strength along the shear plane, to form the chip. This deformation process generates large amounts of heat and is referred as the primary shear zone. As the chip slides on the rake face, the chip continues to deform as well as overcome the frictional forces at the tool-chip interface, generating a secondary source of heat and is referred as the secondary shear zone. The final source of heat generation is due to the friction at the tool-workpiece interface which is in the tertiary shear zone. The heat distribution in the primary, secondary and tertiary zones is shown in Figure 1. The total power consumed during the cutting process is used for the total work done in these three zones [19].

According to the hypothesis made by Trent [20], the total mechanical energy is converted into heat which is distributed in the primary, secondary and tertiary zones as shown in Figure 1. The heat generated at the three shear zones is then dissipated into the chip, tool, and the workpiece.

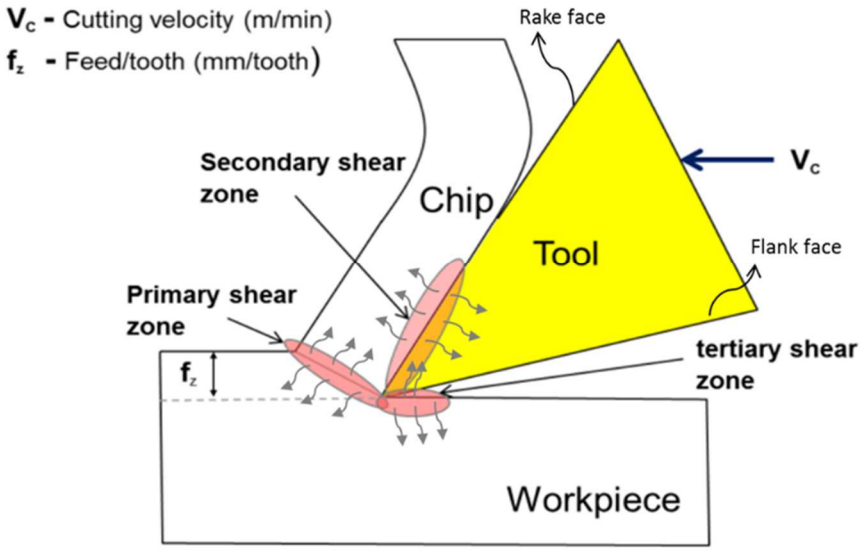

Figure 1 : Heat distribution during machining.

The temperature rise in the tool is due to the heat entering the tool from all of the three sources. Though the secondary heat source is the main cause of temperature rise in the tool, some amount of heat from the primary and tertiary shear zones enters the tool through the tool-chip and tool-workpiece interfaces respectively. The part of the heat entering the tool due to shearing of the workpiece is referred to as ϕ_{Shear} and the part of the heat due to frictional effect i.e generated through the secondary and tertiary shear zones is refered to as $\phi_{Friction}$. Hence the total heat flux generated is given by (Eq. 1).

$$\phi_{Tool} = \phi_{Shear} + \phi_{Friction} \quad (1)$$

It is generally agreed that most of the heat produced due to shear in the primary shear zone is generally removed through the chip and the workpiece material itself [6,21][22]. The heat produced in the secondary and tertiary zones due to the friction enters the tool through the rake and flank face respectively.This is given by the following equation (Eq. 2):

$$\phi_{Friction} = \phi_{rake\ face} + \phi_{flank\ face} \quad (2)$$

Based on this hypothesis, the relationship between the heat flux and the forces at the interfaces could be established. The cutting-edge experiences the forces during the cutting process which is distributed on the rake and the flank faces of the tool. By isolating the tool one can express the resultant force as components of forces on the rake and the flank surface. The friction coefficients, normal and tangential components of forces are required to determine the total heat flux generated due to friction in the secondary and the tertiary shear zones. From the works of Bonnet [23] one can deduce an expression of thermal heat flux in the contact zones which is represented in (Eq. 3).

$$\phi_{Friction} = \frac{1}{A_R} N_R \mu_R V_C \beta + \frac{1}{A_F} N_F \mu_F V_C \beta \quad (3)$$

Where N_R, N_F are the normal forces on the rake and flank surface respectively; β is the heat partition coefficient, μ_R and μ_F are the apparent coefficient of friction experienced at the rake and the flank surfaces; V_C is the cutting speed; A_R and A_F are the contact surface areas at rake and flank face respectively where the heat exchange takes place. It should be noted that same contact velocities and heat partition coefficients are considered for both the rake and the flank surface of the tool as only low finishing condition will be considered in this study. Moreover the study focuses on the influence of the workpiece material i.e conventional laminated Ti6Al4V and EBM – Ti6Al4V at the contact at secondary and tertiary shear zones.

2.2 Hybrid method

With the hybrid approach, one can not only determine the heat flux entering the tool but also understand the phenomenon of tool wear. As explained in the previous section the source of heat flux could be at the primary, secondary and the tertiary shear zones. The heat flux generated in the secondary and the tertiary shear zone due to the cutting forces during the milling test is estimated by this hybrid approach. The hybrid approach utilizes both milling and tribological tests (pin on disc) to estimate the heat flux transmitted into the cutting tool. The phenomenon of wear can be studied to reveal the complex physics behind the wear.

During the milling step, the cutting forces generated and the temperature rise at a certain distance from the cutting edge is measured. To determine the heat flux experienced at the rake and flank surfaces of the tool, apparent coefficient of friction (μ_{app}) and heat partition coefficient (β) are required. This is evaluated using a pin on disc sliding tests. However, the

average sliding velocity at the contact in the rake and the flank face of the tool is assumed to be the same as the cutting velocity. The sliding and sticking zones in the rake surface of the tool as found in the literature are not considered separately [18][22]. The focus of the study is primary to understand the average effect of the material being machined in the heat generation at the contact by using two different experimental set-ups i.e milling and pin-on-disc. The methodology is shown in Figure 2.

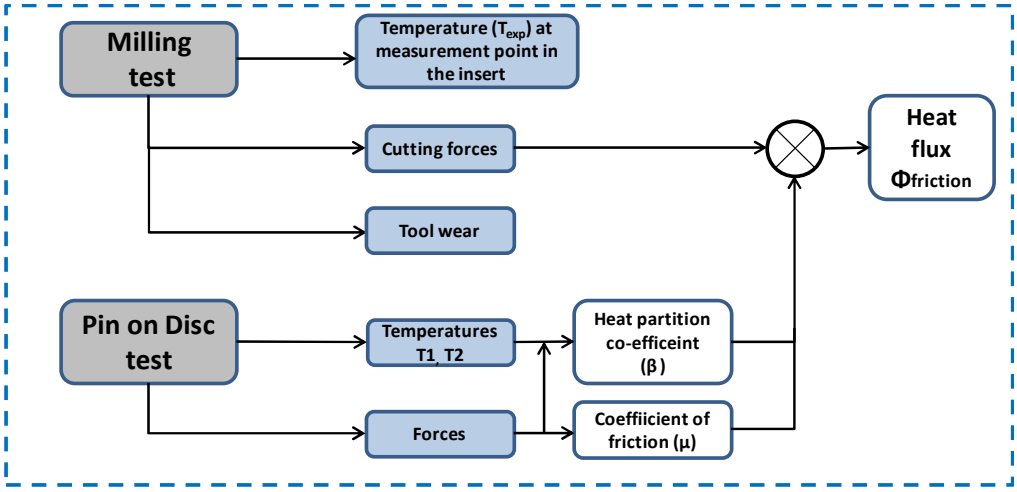

Figure 2 : Schematic representation of Hybrid method.

3. Material fabrication and Experimental setup

3.1 Sample fabrication and heat treatment

Sample dimensions for milling tests with temperature measurements were fixed to be 70×10×10 mm and those for tool lifetime tests to be 200×200×20 mm. Ti6Al4V was produced using Arcam A2 EBM machine with standard 50-micron layer parameters provided by Arcam. In the EBM process, a voltage of 60 kV and electron beam size of ~200μm was used during the melting cycle. The build chamber was kept under vacuum at 2×10^{-3}mbar, controlled using helium as a regulating gas. The powder bed is preheated and maintained at around 800°C using 3kW unfocused e-beam. After preheating, the outer contour is melted using 40 simultaneous multi-spots (340mm/s) then the inner contour using 15 simultaneous multi-spots (800mm/s) and then the core using a raster kind melting strategy. The length of the EBM samples were built along the vertical direction (Figure 3). These samples were then

subjected to a HIP (Hot Isostatic Pressing treatment) at 950°C and 1020 bars for 3 hours to reduce the levels of porosity that might have occurred during the fabrication process.

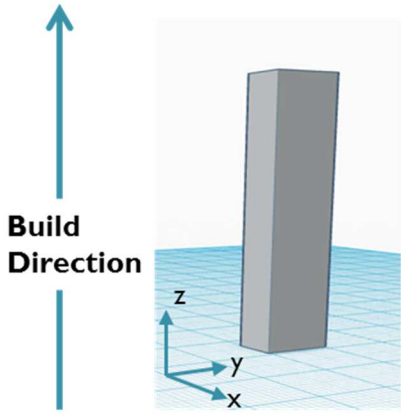

Figure 3 : Build direction of the EBM-Ti6Al4V samples.

3.2 Microstructure

The specimens were sliced along the cross-sectional area for microstructural investigation. The cut samples were mechanically polished up to 1μm with jewel suspension and then scratched with the Kroll's reagent to examine the microstructure. The optical micrographs of the microstructure for the conventionally produced and EBM sample are shown in Figure 4.a and Figure 4.b respectively. The conventional samples have an equiaxed α and α+β structure in which there are extended grains along the rolling direction. The average grain size was 12.5μm. The EBM microstructure has a fine α lamellar grains along with different morphologies including grain boundary of α grains. The average α grain width was 2.5 μm. These differences are mainly attributed to the process routes and parameters used during the fabrication of the samples. This variation in the grain structures is attributed to the different heating and cooling rates during processing. The pre-heating done during the EBM process helps in maintaining a higher process temperature and reduce the cooling rates. Moreover, the heated base plate maintains a temperature around 700°C which could lead to further evolution of the grain morphologies.

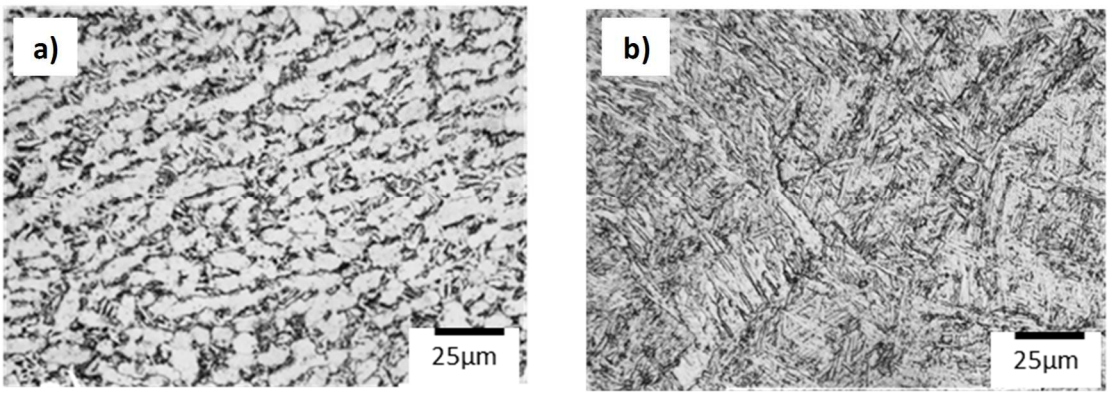

Figure 4 : The microstructure of the (a) Reference-Ti6Al4V and (b) EBM-Ti6Al4V samples.

3.3 Milling test

The tests were performed on *DeckelMaho DMU 60T*, a three-axis milling center. The samples fabricated as parallelepipeds using EBM processes were then machined to a dimension of 70 mm × 10 mm × 5mm. The samples were mounted on a specially designed fixture that could be mounted on a KISTLER dynamometer table (type *9255B*) which was used to measure the forces in the three orthogonal directions F_x, F_y,and F_z. The milling tool Sandvik Coromant-Coromill R300, a 42 mm diameter; neutral axial and radial design with a reference *R 300-42T16-10H* was used. Round inserts with 10 mm diameter with a reference *R300-1032E-PL 1010*, an AlTiN - PVD coated carbide insert grade were used. Radial engagement of the tool was the sample width of 10 mm and the mill was in a central position. The machining was done in dry condition. The cutting conditions used during the milling tests are given in Table 1. However, the purpose of this study is to identify the effects of using these conditions on the thermal behavior of the tool while finish milling of the same alloy produced by the EBM process. The tests were repeated three times and mean value is used for the analysis.

Table 1: Cutting conditions of the milling process.

Cutting speed (V_c)	55 m/min
Feed rate (f_z)	0.1 mm/rev
Depth of cut (a_p)	1 mm
Engagement (a_e)	27%

The temperature rise was measured by wireless thermocouple equipment developed by *ATCOM*. The transmitter (*ATE4TH*) and the receiver (*ATR6ACU* 433MHz version) users can

record up to 4 simultaneous signals at a frequency of 8 Hz (Figure 5). A specially designed adaptor along with a plastic housing was used between the HSK 63 coupling and the tool holder which holds the components of the thermocouple equipment. A hole with a diameter ⌀1mm was drilled behind the insert so that we could introduce the thermocouple in order to measure the temperature rise in the insert close to the cutting zone. Figure 5(b) shows the plan of the insert with the hole where thermo-couple will be introduced. The hole was made using electro-erosion process and the depth was controlled with optical 3D profiling to ensure the tolerance of ±0.05 mm with all the inserts used during the test. All the tests were repeated thrice to ensure repeatability of the measurements.

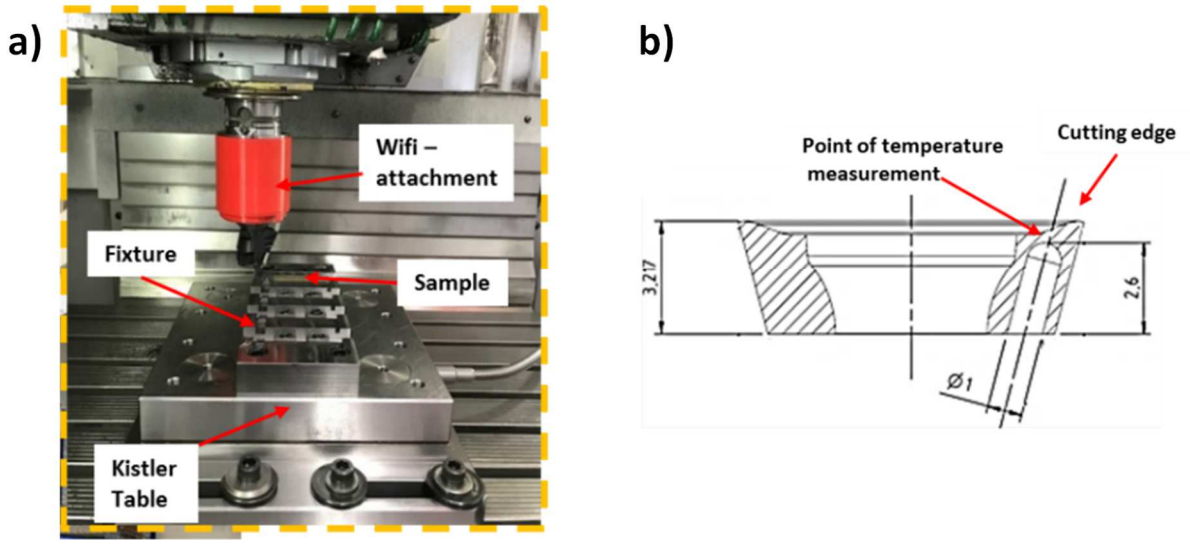

Figure 5 : Experimental Setup to measure temperature and forces while milling operation .

3.4 Pin on disc test

The Ti6Al4V discs made with the reference material and EBM process had a diameter of 100 mm. The disc made by EBM process was constructed in the vertical direction (diameter along the Z direction of the machine) with the same process parameters that were used to produce the samples made for the machining test. The EBM disc was also HIPed with the same conditions as the sample used for the milling test.

The pin has a dimension of 8 mm diameter and 12 mm hemispherical head. They are made of the tungsten carbide grade 902 and then PVD coated with a 3μm *AlTiN* - which is the same as that of the insert used during the milling tests. The surface of the pin is polished to have a

roughness of $Ra < 0.2\ \mu$m. The pin was made to slide over the disc made up of the workpiece material. To operate the test in an open configuration i.e. to have a renewed surface as the pin slides over the disc, a spiral trajectory is used. The normal force, F_n is applied on to the pin. When the disc starts to rotate, it generates a tangential component, F_t which can be measured with the dynamometer fixed on the support that holds the pin. This gives the apparent coefficient of friction μ_{app} defined by the relation (Eq. 4).

$$\mu_{app} = \frac{F_t}{F_n} \tag{4}$$

The tribometer set-up used in the study shown in Figure 6. The tests were realized on an NC Victor V-turn A26 turning machine. The pin is mounted on a specially designed fixture that is attached to a KISTLER type *9129AA* dynamometer table. The radial displacement of the pin is along the X-axis of the turning machine. The disc is mounted on the chuck and RPM is controlled using G96 code to maintain a constant surface speed (CSS). CSS is needed to maintain a constant relative velocity between the pin and the rotating disc by changing the RPM as the pin moves along the X-axis. This generates a spiral sliding path on the surface of the disc thus enabling the tribometer to operate under open configuration i.e. the pin slides over a new surface every time. The normal and the tangential forces on the pin during sliding were measured at a frequency 3000 Hz during the sliding tests.

Heat partition coefficient between the tool-workpiece pair is estimated by calculating the flux entering the pin and the total power consumed by the sliding test due to friction. This is estimated by measuring the temperature gradient and heat flux in the pin. The temperature gradient in the pin was measured using two thermocouples (Figure 6-b). Thermocouples were introduced into 1mm diameter drilled holes spaced at an interval of 3 mm distance. The *K* type thermocouples used were of 0.13 mm diameter and were connected to National Instruments NI USB-9162 equipment. Labview Signal Express software was used to record the temperature at a frequency of 3 Hz.

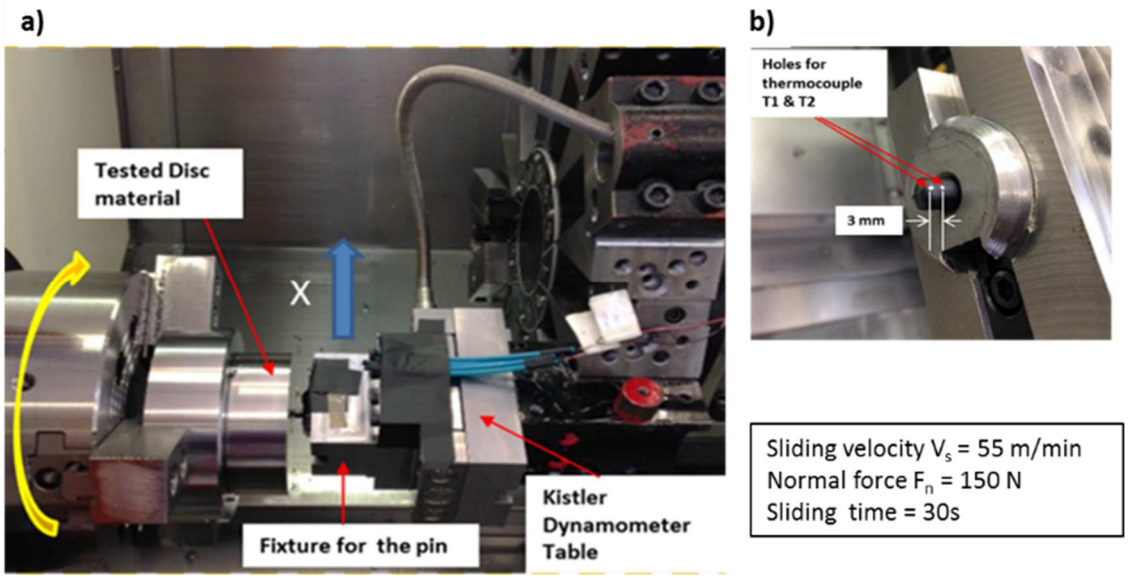

Figure 6 : Pin on Disc experimental set up.

4. Results and discussion:

4.1 Milling test

4.1.1 Cutting forces

The cutting forces measured during the milling test were measured by the fixed reference frame of the dynamometer table. The measured forces in the three orthogonal directions are shown in Figure 7. The EBM Ti6Al4V produced 10% higher force when compared to the reference alloy. The higher forces observed is justified by the fine microstructure of the EBM Ti6Al4V due to the higher cooling rates that exist while fabrication process [24]. The difference in the forces is due to differences in the shear strength and the frictional effects at the tool-chip and tool-workpiece interfaces. Nevertheless, these forces must be distributed along the rake and the flank surfaces of the insert for estimating the heat flux that could be generated on the tool-chip and tool-workpiece contact surfaces. The *section 4.1.2.* demonstrates the components of forces on the rake and the flank surfaces.

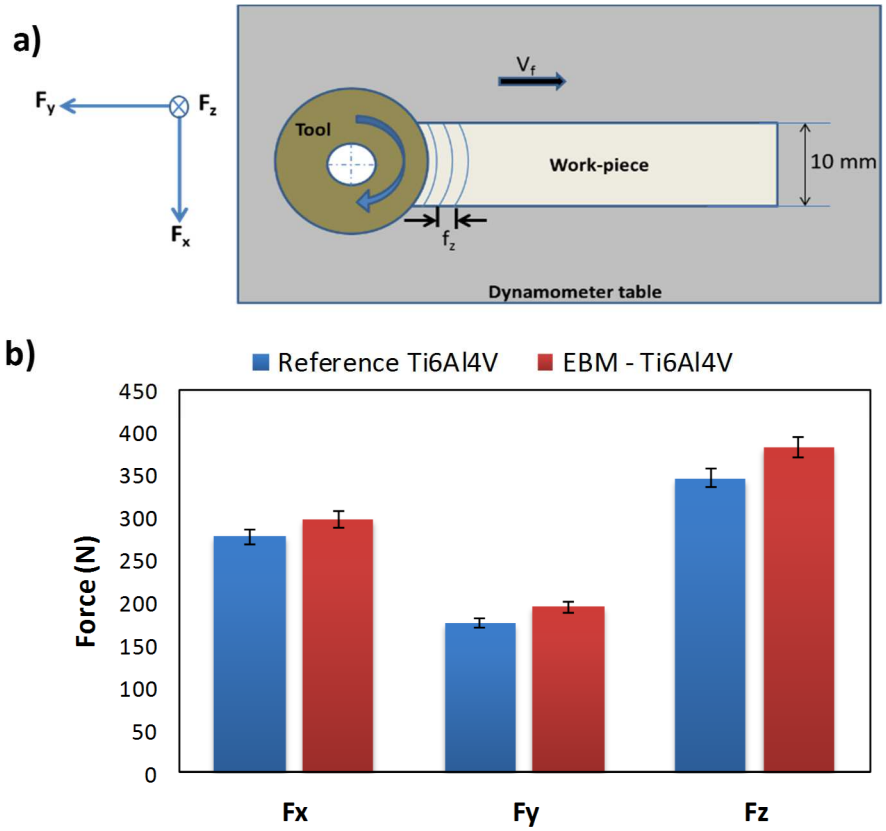

Figure 7 : a) Representation of orthogonal components of force during milling and (b) Measured forces for reference and EBM Ti6Al4V.

4.1.2 Determining the normal forces on the cutting edge

To determine the forces experienced at the cutting edge i.e. at the rake and the flank faces of the insert, the reference frame must be transformed. This reference transformation represented in Figure 8. The change of reference frame is done to include the rotation of the tool and the geometrical angles of the tool and insert's cutting edge. Based on the inserts geometry and the milling parameters, the insert entering angle (K_r) would change. The entering angle for a round insert is calculated using the feed rate f_z and maximum chip thickness H_{ex}: which is given by (Eq. 5).

$$\sin K_r = \frac{H_{ex}}{f_z} \tag{5}$$

Where H_{ex} is given by the following relation (Eq. 6)

$$H_{ex} = \frac{2.f_z.\sqrt{a_p.d - {a_p}^2}}{d} \tag{6}$$

The normal forces experienced at the two surfaces are calculated with the orthogonal components of the cutting force along with the geometric angles of the tool and the insert. The effective rake angle, γ_n considering both the tool and the insert geometry is -7° in our case.

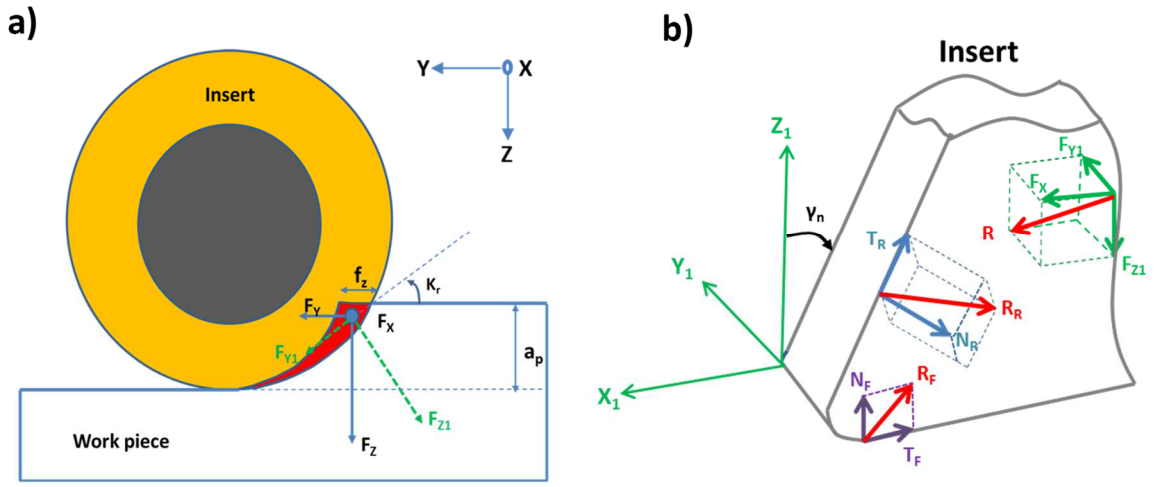

Figure 8 : Representation of cutting forces on the cutting edge taking in to account a) insert entering angle (K_r), b) effective rake angle, γ_n.

By the principle of equilibrium of forces at the cutting edge, one can deduce the value of the normal forces N_R and N_F on the rake and the flank face of the tool respectively as shown in the (Eq. 7) and (Eq. 8). Here the coefficient of friction is considered to be constant and is taken as μ on the rake and the flank surfaces for simplification. It should be noted that this is an approximation and the value of the calculated heat flux will not take into account the effect of local pressures which is an essentially not constant along the chip-tool and tool-workpiece contact surfaces.

$$N_R = \frac{F_{Z1}.\mu - F_X}{\mu(\cos\gamma_n.\mu - \sin\gamma_n) - \sin\gamma_n.\mu - \cos\gamma_n} \tag{7}$$

$$N_F = \frac{(\cos\gamma_n.F_X - \sin\gamma_n.F_{Z1}).\mu - \cos\gamma_n.F_{Z1} - \sin\gamma_n.F_{Z1}}{\mu(\cos\gamma_n.\mu - \sin\gamma_n) - \sin\gamma_n.\mu - \cos\gamma_n} \tag{8}$$

The contact surface area where the heat exchange had taken place on the insert is estimated by observing the sliding zones under scanning electron microscope. The results are summarized in Table 2.

Table 2: Contact surface areas on the insert after milling tests.

Sample	Rake surface, A_R ($\times 10^{-8}$m²)	Flank surface, A_F ($\times 10^{-8}$m²)
Reference-Ti6Al4V	26.2	10.2
EBM-Ti6Al4V	25.3	10

It can be noted that the contact areas were slightly lower in the case of EBM-Ti6Al4V sample. The effective zone of heat transfer influences the heat flux density which could affect the maximum temperatures that could be attained at the cutting edge.

Once the apparent coefficient of friction and the heat partition coefficient are determined, one can predict the heat flux entering the tool with the Equation 3. The results of the heat flux estimation are discussed in section 4.3.

4.1.3 Temperature rise while milling

Figure 9 shows an example of the evolution of cutting tool temperature measured while milling the EBM-Ti6Al4V and reference Ti6Al4V. As the temperature rise as measured at about 0.6 mm from the cutting edge (see Figure 5-c), a quasi-steady state temperature is achieved after 10 seconds' in both the cases. The data points of the measured temperature are fitted by least square method, with an exponential curve as a function of time 't': y(t)= $Ae^{-B/t} + T_{ambient}$. The solid lines in the Figure 9 shows the fitted curve. The maximum temperature measured after the 25 seconds of machining the EBM Ti6Al4V is found to be around 100°C whereas in the case of the reference Ti6Al4V it was 80°C.

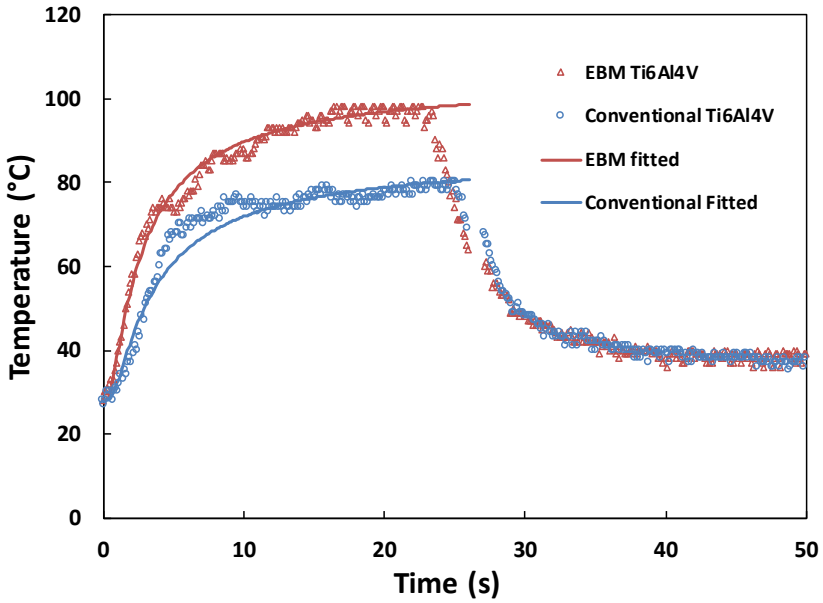

Figure 9 : Example of evolution of temperature while milling EBM Ti6Al4V and reference Ti6Al4V

This clear difference in the rise in temperature is an indication of the levels of heat flux that enter the tool are different depending on the microstructure along with the mechanical and the tribological properties at the tool-chip and tool-workpiece interface. The maximum cutting edge temperatures corresponding to the measured would be much higher, and could be determined by using inverse numerical method [6,12]. The cutting edge temperatures could be as high as 1000°C while machining Ti alloys [19,20]. However, the effect of such differences in temperatures would influence the wear mechanism and could be understood by performing tool lifetime tests.

4.2 Pin on disc test

4.2.1 Variation of apparent coefficient of friction

The normal force used for the sliding test was 150 N. This was used to have a contact pressure similar to the case of machining which was found to be about 1.5 GPa based on Hertzian contact theory. Contact pressures between 1 to 3 GPa are expected at the contact conditions during machining and are usually determined using numerical simulations [22]. The sliding velocity was the same that in the case of milling which is 55 m/min. The sliding distance was 20 meters for each test to ensure that the forces were measured after a quasi-steady state is attained. Figure 10 shows the variation of the apparent coefficient of friction

attained using the EBM-Ti6Al4V and reference-Ti6Al4V discs. Lower coefficient of friction was observed in the sliding tests with EBM-Ti6Al4V. To understand this behavior the wear surfaces on the pin were examined.

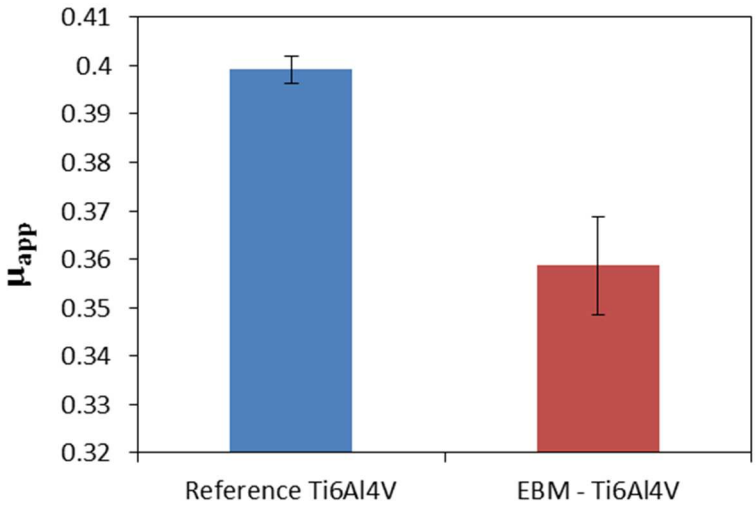

Figure 10 : Variation of apparent coefficient of friction μapp in for sliding tests on reference-Ti6Al4V and EBM-Ti6Al4V.

Figure 11 shows one of the SEM images of the wear surfaces of the pin slid over the reference-Ti6Al4V and EBM-Ti6Al4V discs. It can be noted that levels of adhesion on the pins are clearly different and lower volume adhesion material was observed in the case of EBM disc when compared to that of the reference Ti6Al4V disc. The lower volumes of the adhesion layer could be related to the microstructural differences to a certain extent by different morphology as well as $\alpha + \beta$ phase distribution [25]. In our case the EBM samples have an acicular morphology of the α grains with very negligible amount of β phases present, whereas the reference samples have an equiaxed α + β morphology. The lower adhesion material in the case of EBM sample would justify the lower contact area and lower tangential forces which result in a lower apparent coefficient of friction.

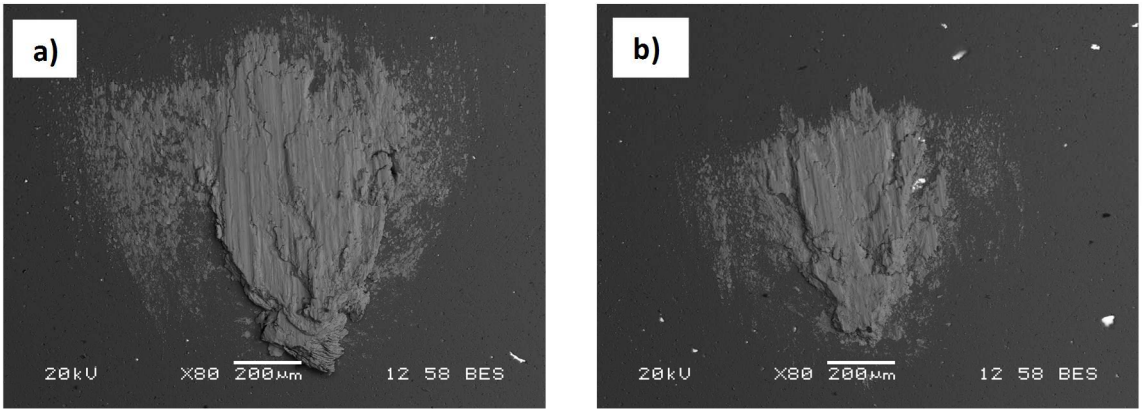

Figure 11 : Adhesive material on the pin after sliding on a) Reference-Ti6Al4V, b) EBM-Ti6Al4V

4.2.2 Heat partition

The heat flux generated at the pin-disc interface due to the effects of friction caused by the sliding action of the pin over the disc. During the sliding test, the heat flux entering the pin (tool material) denoted by Φ_{pin} was calculated using the temperature gradient, ΔT measured using two thermocouples *T1* and *T2*. Figure 12 shows an example of the temperature curves recorded by thermocouples while sliding test on EBM-Ti6Al4V disc.

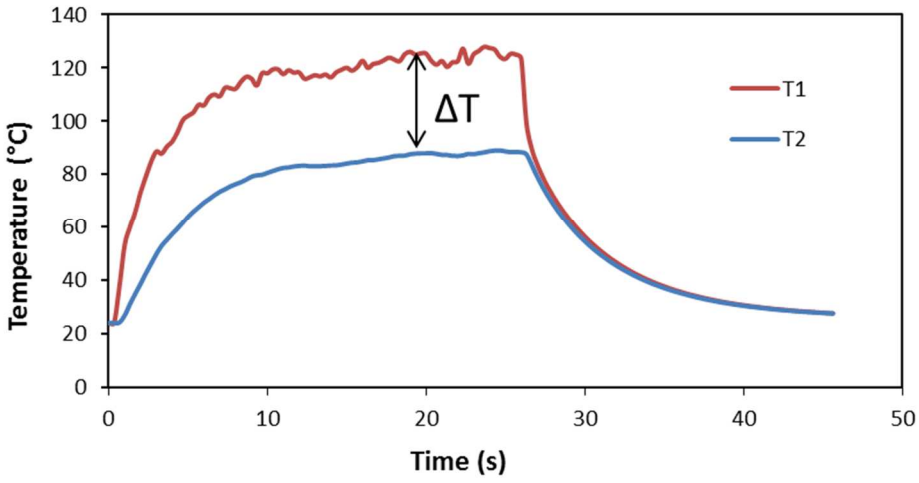

Figure 12 : Example of evolution temperature in the pin in thermocouples T1 and T2 while sliding on EBM Ti6Al4V disc.

Assuming that whole of the frictional power is converted to heat that is being dissipated into the two bodies at contact, using the Fourier's law in steady state, the heat flux passing through the pin is given by (Eq. 9).

$$\Phi_{pin} = k \times S_{pin} \times \frac{\Delta T}{dx} \quad (9)$$

Where k is the thermal conductivity of the pin (89 W/m.K at 100°c),

S_{pin} is cross sectional area of the pin (50mm²),

$\Delta T/dx$ is the temperature gradient in the pin.

The global power consumed by friction tests can be estimated by the following expression (Eq. 10).

$$P_{total} = F_t \times V_s \quad (10)$$

Where F_t is apparent tangential force and V_s is sliding velocity.

The ratio of the heat flux entering the pin to the total power consumed by friction gives the heat partition coefficient given by the (Eq. 11).

$$\beta_{pin-disc} = \frac{\Phi_{pin}}{P_{total}} \quad (11)$$

Table 3 summarizes the results of the pin on disc test. It can be observed that the heat partition coefficient calculated for the sliding on the EBM-Ti6Al4V disc is 0.947 whereas in the case of the reference Ti6Al4V disc is 0.648. This means that most of the heat generated at the pin-disc interface enters the tool. This could again be explained by the phenomenon of adhesion observed at the interface. The volume of the adhered material at the interface could be considered as a third body at the contact during the sliding action. Though the exact nature of the adhered material is to be questioned, in our case it is mainly the wear particles generated from the disc which is the alloy Ti6Al4V itself. As this layer of adhered material is of very low thermal conductivity (about 7 W/m.K), the effective transfer of heat from the contact pairs i.e. the pin and the disc could be low. Moreover, the part of the heat generated due to friction is used to keep the adhered material sticking on to the pin itself [26]. This explains the higher heat transferred into the pin while sliding on the EBM-Ti6Al4V disc. Taking into account the factors such as coefficient of friction, heat partition and the levels of adhesion with this hybrid method, one can precisely study the effect of the temperature rise in the degradation of the tool. This will be further studied using actual milling tests and will be discussed in the *section 5.1.*

Table 3.Results of the pin on disc test for EBM Ti6Al4V and reference Ti6Al4V.

Disc	***Ft (N)***	μ_{app}	$\Delta T(°C)$	$\Phi_{pin}(W)$	P_{total} **(W)**	$\beta_{pin\text{-}disc}$
Reference Ti6Al4V	63,15	0.42	25.5	37.56	57.88	0.648
EBM-Ti6Al4V	54,3	0.36	32	47.14	49.77	0.947

4.3 Heat flux estimation

As described in earlier *section 2*, the heat flux entering the tool is now calculated with the normal forces on the rake and flank faces of the tool from the milling tests along with the apparent coefficient of friction and the heat partition coefficient determined from the pin on disc tests. Thermal power is calculated with respect to the contact areas A_R and A_F at the rake and flank surfaces respectiviely (Table 4). In the case of EBM-Ti6Al4V, about 55% higher heat flux enters the tool for similar conditions of machining. This higher heat flux entering the cutting tool will lead to higher temperatures at the cutting edge. This is important as the properties like shear strength and wear resistance of the cutting tool depends on the maximum temperature attained at the cutting edge [27].

Table 4. Estimation of normal forces, heat flux, and thermal power for EBM-Ti6Al4V and Reference-Ti6Al4V.

Sample	N_R (N)	N_F(N)	ϕ_{Friction} (W/mm²)	Thermal Power (W)
Reference-Ti6Al4V	190.6	260.08	800	110.2
EBM-Ti6Al4V	206.1	299.2	1240	167.2

5. Discussion

In this study the thermal effects due to machining the EBM Ti6Al4V has been studied with respect to the heat flux generated along with the heat partition and the adhesion phenomenon occurring during the tool-material interaction at the contact. There is a significant difference in the levels of adhesion between the EBM Ti6Al4V and the reference Ti6Al4V for similar conditions of sliding which leads to the difference in the heat partition as we have seen

previously. However, to establish a strong correlation between the observations made in the pin on disc set up with the actual milling test and to study the effect on the tool wear further machining tests were done as discussed below.

5.1 Effect of temperature rise on tool life

Milling tests were done to estimate the tool life of the insert and to plot the evolution of the tool wear with machining time. Solid blocks of the workpiece material were used for these tests. The samples were built with the same build parameters as mentioned in previously and then HIPed before milling them. The same cutting conditions shown in Table 1 was used for the lifetime tests. The evaluation was done in terms of flank wear and the tests were repeated twice. Figure 13 shows the results of evolution of the flank wear (V_b) were compared to that of the reference Ti6Al4V. The tool life criteria was set to be a maximum flank wear of 0.3 mm according to the ISO3685 standards [28]. It can be noted that the tool wear is uniformly progressive while machining the reference-Ti6Al4V whereas for the EBM-Ti6Al4V the wear is accelerated with a steep slope as shown in Figure 13. The tool reaches the maximum flank wear after 24 minutes in the case of EBM-Ti6Al4V whereas for the reference-Ti6Al4V the tool endures upto 55 minutes.

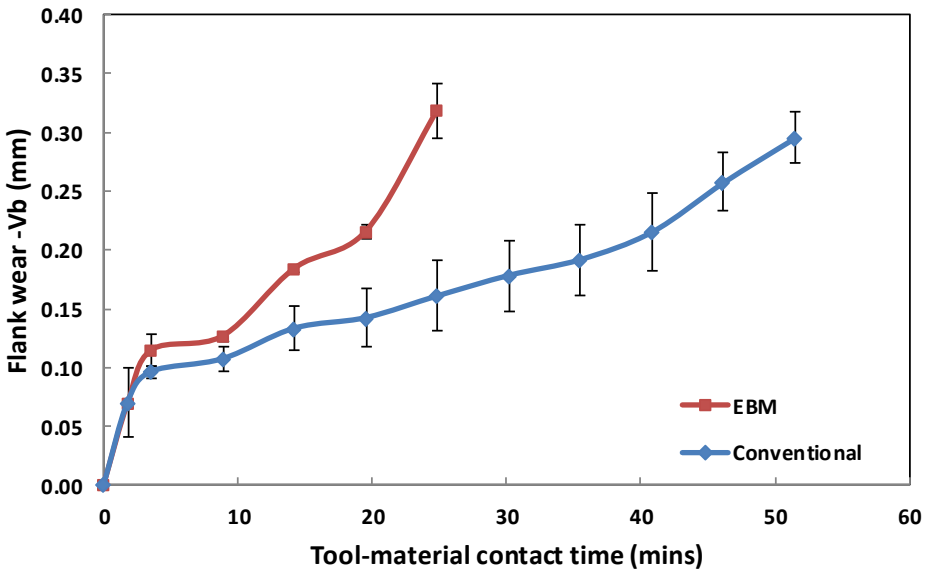

Figure 13 : Evolution of flank wear while milling EBM-Ti6Al4V and reference-Ti6Al4V.

At lower cutting sp eed (less than 60 m/min), adhesive and abrasive wear are dominant while machining Ti6Al4V with coated WC tools [29]. Delamination of the coating occurred at the very early stage (within 5 mins) of machining in both the cases. It means that new

surface of WC is exposed and leads to adhesion of workpiece material [30]. To study the worn tool SEM micrographs were taken after machining the EBM and Reference Ti6Al4V. Figure 14 shows the backscatter images of the cutting edge. It can be observed that the extent adhesive layer formed on the cutting edge is irregular for EBM-Ti6Al4V when compared to reference Ti6Al4V. The regions of white contrast show the raw substrate material of the tool. This is confirmed by the EDAX analysis at point 'P' in Figure 14-b. Loss of material leading to theformation of a crater could be observed in the case of EBM-Ti6Al4V. This uneven wear could be attributed to the removal of tool material along with the strongly bonded adhered work-piece material. Stronger bonds could be a result of attrition and diffusion mechanisms which could form TiC bonds (Eq. 12) which is verified with Gibb's free energy reaction [31].

$$WC + Ti \rightarrow TiC + W \tag{12}$$

This difference in wear mechanism is attributed to the higher temperatures that could be attained at the tool-chip and tool-workpiece interface while machining EBM-Ti6Al4V.

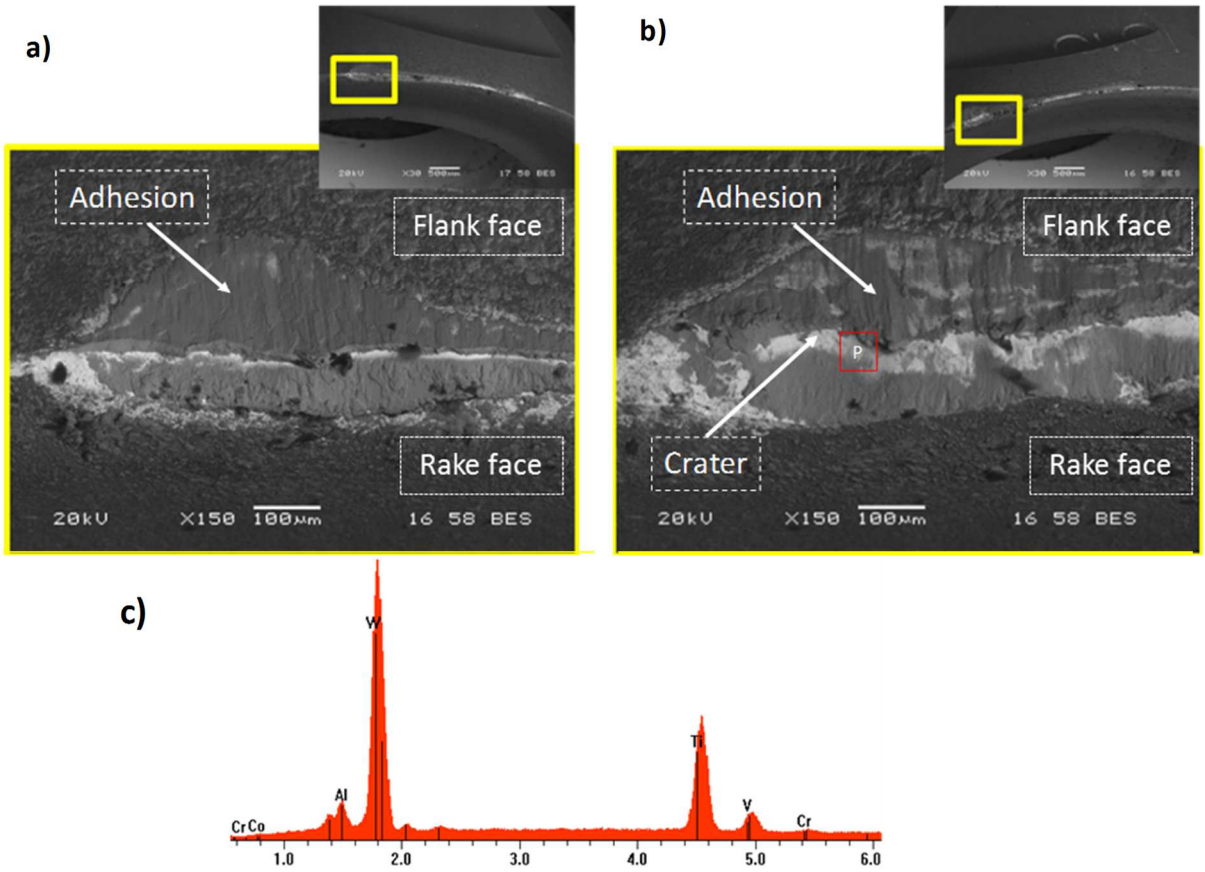

Figure 14 : Backscatter Images of Worn cutting edges at the end of tool life (Vb = 0.3 mm) after machining (a) Reference Ti6Al4V, (b) EBM – Ti6Al4V, (c) EDAX analysis at point P showing a high concentration of tungsten (W) of the substrate.

The effect of temperature rise on the tool life time and the wear mechanisms is established for the EBM Ti6Al4V. The study is based on the hybrid approach of combining the milling and pin on disc tests helped in understanding the complex thermo-mechanical phenomena in terms of distribution of forces, apparent coeeficeint of friction, heat partition at the contact and heat flux entering the tool. The lower tool life while machining EBM Ti6Al4V is due to the lower levels of adhesion and higher heat partition into the tool. This hybrid approach has helped in quantifying different thermal and mechanical properties at the tool-material contact and in turn understand the primary wear mechanisms leading to lower tool life while milling EBM Ti6Al4V.

6. Conclusions

The effect of the temperature rise while milling EBM-Ti6Al4V has been studied with a hybrid method. This study involved both milling and tribological tests to estimate the heat flux entering the cutting tool. The higher heat flux generated while milling EBM-Ti6Al4V is due to a combination of several factors.

The following conclusions can be made based on this study

- The cutting forces are higher while milling EBM Ti6Al4V due to its higher shear strength and finer microstructure when compared to the reference-Ti6Al4V. The temperature rise in the cutting tool was also higher for the EBM-Ti6Al4V.
- The frictional behavior at the tool-chip and tool-workpiece material was found to be dependent on the adhesion mechanisms which influenced the quantity of the material adhered to the tool. This was confirmed with the pin on disc experiments where lower apparent coefficient of 0.36 was found for the EBM-Ti6Al4V. Moreover, the heat partition coefficient was found to be inversely proportional to the adhesion volume. This is explained by the concept of the third body at the sliding interface which essentially has a lower thermal conductivity.
- It is clear that the temperature rise in the tool depends on the wear behavior of the EBM-Ti6Al4V. The lower levels of adhesion have actually been found to deteriorate the tool by exposing a new surface in contact as the tool begins to wear. In the case of the reference-Ti6Al4V the adhesion layer forms a kind of thermally insulating coating and hence the new surface of the tool is not exposed to frictional encounter with the

chip of the workpiece surface. Tool lifetime test showed a 50% reduced tool life when compared to milling the reference -Ti6Al4V.

Considering the effect of temperature on the wear mechanisms, it is important to determine the maximum cutting edge temperatures to identify if it is high enough to affect the mechanical behavior of the WC tool. The predicted heat flux can be used for an inverse numerical analysis for this purpose. The effect of different tool coatings could change the thermal phenomenon at the tool-workpiece material contact. This will be the focus in the future research. There is a larger scope to develop new coatings to resist the heat flow and to modify the wear mechanism while machining EBM-Ti6Al4V and to ensure higher productivity. This will be investigated in the future works.

7. References

[1] Rawal S, Brantley J, Karabudak N. Additive manufacturing of Ti-6Al-4V alloy components for spacecraft applications. RAST 2013 - Proc 6th Int Conf Recent Adv Sp Technol 2013:5–11. doi:10.1109/RAST.2013.6581260.

[2] Dutta B, (Sam) Froes FH. The additive manufacturing (AM) of titanium alloys. Elsevier Inc.; 2015. doi:http://dx.doi.org/10.1016/B978-0-12-800054-0.00024-1.

[3] Townsend A, Senin N, Blunt L, Leach RK, Taylor JS. Surface texture metrology for metal additive manufacturing: a review. Precis Eng 2016;46:34–47. doi:10.1016/j.precisioneng.2016.06.001.

[4] Veiga C, Davim JP, Loureiro AJ. Review on Machinabality of Titanium Alloys: The Process Prespective. Rev Adv Mater Sci 2013;34:148–64.

[5] Ezugwu E WZ. Titanium alloys and their machinability – a review. J Mater Process Technol 1997;68:262–74.

[6] Davies, M. A., T. Ueda, R. M'Saoubi, Davies, M. A., T. Ueda, R. M'Saoubi, B. Mullany ALC. On The Measurement of Temperature in Material Removal Processes 1. Ann CIRP 2007;56:581–604. doi:10.1016/j.cirp.2007.10.009.

[7] Kikuchi M. The use of cutting temperature to evaluate the machinability of titanium alloys. Acta Biomater 2009;5:770–5. doi:10.1016/j.actbio.2008.08.016.

[8] Che-Haron CH, Jawaid A. The effect of machining on surface integrity of titanium alloy Ti-6% Al-4% v. J Mater Process Technol 2005;166:188–92. doi:10.1016/j.jmatprotec.2004.08.012.

[9] T. Kitwaga, A. Kubo, Maekawa K. Temperature and wear of cutting tools in high-speed machining of Incone1718 and Ti-6A1-6V-2Sn. Wear 1997;202:142–8.

[10] Kagnaya T, Lazard M, Lambert L, Boher C, Cutard T. Temperature evolution in a WC-6 % Co cutting tool during turning machining : experiment and finite element simulations. WSEAS Trans HEAT MASS Transf 2011;6:71–80.

[11] Lazard M, Corvisier P. Modelling of a tool during turning Analytical prediction of the temperature and of the heat flux at the tool Õ s tip. Appl Therm Eng 2004;24:839–49. doi:10.1016/j.applthermaleng.2003.11.007.

[12] Kagnaya T, Boher C, Lambert L, Lazard M, Cutard T. Wear mechanisms of WC – Co cutting tools from high-speed tribological tests. Wear 2009;267:890–7. doi:10.1016/j.wear.2008.12.035.

[13] Kus A, Isik Y, Cemal Cakir M, Coşkun S, Özdemir K. Thermocouple and infrared sensor-based measurement of temperature distribution in metal cutting. Sensors (Switzerland) 2015;15:1274–91. doi:10.3390/s150101274.

[14] Korkut I, Boy M, Karacan I, Seker U. Investigation of chip-back temperature during machining depending on cutting parameters. Mater Des 2007;28:2329–35. doi:10.1016/j.matdes.2006.07.009.

[15] Zemzemi F, Rech J, Salem W Ben, Dogui A, Kapsa P. Identification of a friction model at tool / chip / workpiece interfaces in dry machining of AISI4142 treated steels. J Mater Process Tech 2008;9:3978–90. doi:10.1016/j.jmatprotec.2008.09.019.

[16] Hedenqvist P, Olsson M. Sliding wear testing of coated cutting tool materials. Tribol Int 1991;24:143–15.

[17] Bonnet C, Valiorgue F, Rech J, Claudin C, Hamdi H, Bergheau JM, et al. Identification of a friction model — Application to the context of dry cutting of an AISI 316L austenitic stainless steel with a TiN coated carbide tool. Int J Mach Tools Manuf 2008;48:1211–23. doi:10.1016/j.ijmachtools.2008.03.011.

[18] Rech J. Influence of cutting tool coatings on the tribological phenomena at the tool – chip interface in orthogonal dry turning. Surf Coat Technol 2006;200:5132–9. doi:10.1016/j.surfcoat.2005.05.032.

[19] Grzesik W. Heat in Metal Cutting. Adv. Mach. Process. Met. Mater., Elsevier B.V.; 2017, p. 163–82. doi:10.1016/B978-0-444-63711-6.00009-0.

[20] E.M. T. Metal Cutting. London: 1991.

[21] Lazoglu I, Altintas Y. Prediction of tool and chip temperature in continuous and interrupted machining. Int J Mach Tools Manuf 2002;42:1011–22.

[22] Bonnet C, Valiorgue F, Rech J, Hamdi H. Improvement of the numerical modeling in orthogonal dry cutting of an AISI 316L stainless steel by the introduction of a new friction model. CIRP J Manuf Sci Technol 2008;1:114–8. doi:10.1016/j.cirpj.2008.09.006.

[23] Bonnet C. Comprehensive study of cutting phenomena for Titanium alloys Ti6Al4V and CFRP stacks drilling in dry condition. Arts et M{é}tiers ParisTech, 2010.

[24] AL-BERMANI SS, Blackmore ML, Zhang W, Todd I. The Origin of Microstructural Diversity , Texture , and Mechanical Properties in Electron Beam Melted Ti-6Al-4V. Metall Mater Trans A 2010;41:3422–3434. doi:10.1007/s11661-010-0397-x.

[25] Sikorski ME. Correlation of the Coefficient of Adhesion With Various Physical and Mechanical Properties of Metals. J Basic Eng 1963:279–85.

[26] Berthier Y. Consequences and Use of the Third-Body Concept to Solve Friction and Wear Problems. In: Stachowiak G, editor. Wear - Mater. Mech. Pract., John Wiley & Sons, Ltd; 205AD, p. 292–316.

[27] Teppernegg T, Klünsner T, Kremsner C, Tritremmel C, Czettl C, Puchegger S. High temperature mechanical properties of WC – Co hard metals. Int J Refract Met Hard Mater 2016;56:139–44. doi:10.1016/j.ijrmhm.2016.01.002.

[28] International Organization for Standardization, Genève, Switzerland (2003). n.d.

[29] Stephenson, D.A. and Agapiou JS. Metal Cutting Theory and Practices. 2nd ed. Taylor & Francis group; 2006.

[30] Jawaid A, Sharif S, Koksal S. Evaluation of wear mechanisms of coated carbide tools when face milling titanium alloy. J Mater Process Technol 2000;99:266–74.

[31] Pawar P, Joshi S, Tewari A, Joshi S. Tool wear mechanisms in machining of titanium alloys. Int J Mach Mach 2012;2:4–8.

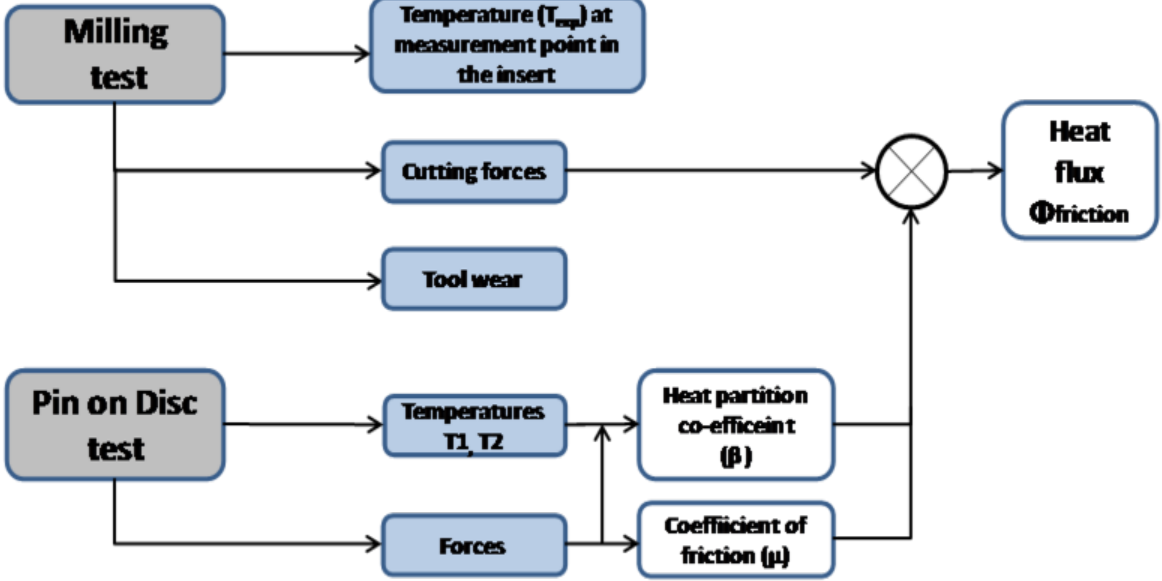
Milling test
Temperature (T_{exp}) at measurement point in the insert
Cutting forces
Tool wear
Heat flux Φfriction
Pin on Disc test
Temperatures T1, T2
Heat partition co-efficeint (β)
Forces
Coeffiicient of friction (μ)